Innovative quartz enhanced photoacoustic sensors for trace gas detection

Vincenzo Spagnolo[*a], Pietro Patimisco[a,b], Angelo Sampaolo[a,b], Marilena Giglio[a], Lei Dong[c], Gaetano Scamarcio[a], Frank K. Tittel[b]

[a]Dipartimento Interateneo di Fisica, Università e Politecnico di Bari, CNR-IFN BARI, Via Amendola 173, Bari, Italy; [b]Department of Electrical and Computer Engineering, Rice University, 6100 Main Street, Houston, TX 77005, USA; [c]State Key Laboratory of Quantum Optics and Quantum Optics Devices, Institute of Laser Spectroscopy, Shanxi University, Taiyuan 030006, China

ABSTRACT

A detailed analysis of the quality factor, the resonance frequency and the electrical resistance of custom quartz tuning forks (QTFs) having different geometrical parameters is reported. We implemented custom QTFs in a quartz enhanced photoacoustic sensor targeting water vapor detection and compared the fundamental and first overtone flexural modes gas sensor performances.

Keywords: Gas Sensing, Quartz tuning fork, photoacoustic spectroscopy.

1. INTRODUCTION

Quartz-enhanced photoacoustic spectroscopy (QEPAS) is an effective technique that allows selective and sensitive measurements of trace gases in an ultra-small acoustic detection module (ADM) with a total sample volume of only a few cm^3 [1-4]. This technique is based on the photoacoustic (PA) effect, where the absorption of the modulated laser radiation by gas molecules causes periodic heating of the chemical species. The heating results in thermal expansion and leads to a pressure change in the targeted trace gas media. In QEPAS systems the generated pressure wave is detected by a quartz tuning fork (QTF) acting as sharply resonant piezoelectric transducer. Most QEPAS sensors reported in the literature use commercial QTFs having a fundamental in-plane flexural mode resonance frequency at ~ 32.76 kHz and characterized by a small volume (prong length L = 3.0 mm, thickness T = 0.35 mm and a typical crystal width w = 0.34 mm) with a prongs spacing of 300 μm. These QTFs were originally designed for time measurements. The prongs geometry and crystal cut were optimized to maintain a selected resonance frequency over a wide temperature range and no optimization of the QTF size and geometry was pursued for trace gas sensing applications. With the aim of determining the dependence of the QTF parameters and performance on their relevant dimensions and identifying the optimal design for optoacoustic gas sensing, we designed QTFs with different values of the spacing between the prongs length, width, and crystal thickness [5].

In this work, we report on the experimental and theoretical analysis of the influence of prongs dimensions on the main physical parameters controlling the QTF performance, namely, the quality factor Q, the resonance frequency and the electrical resistance. To study the acousto-electric transduction efficiency of the custom QTFs, we implemented them in a QEPAS sensor operating in the near-IR spectral range and selected water vapor as the target gas. The QEPAS signals obtained using both the fundamental and the first overtone QTFs flexural modes were compared and demonstrated that, by an optimized design of the QTF prongs, the overtone vibrational modes can provide higher QEPAS signals [6, 7].

2. CUSTOM QUARTZ TUNING FORK

A z-cut quartz wafer with a 2° rotation along the x-axis, which provides stable frequency at room temperature, was selected for the realization of custom QTFs. Standard photolithographic techniques were used to etch the QTFs. Cr and Au patterns were photolithographically defined on both sides of the wafer. A three-dimensional crystal structure is generated by chemical etching in a hydrogen fluoride solution, and finally side electrodes are applied by means of shadow masks [8]. The schematics of the designed QTFs are shown in Fig. 1. In terms of elastic modelling, each prong can be described as a single harmonic oscillator and its motion can be described using a one-dimensional model. The resonance frequencies in vacuum are given by [9]:

Optical Sensing and Detection IV, edited by Francis Berghmans, Anna G. Mignani, Proc. of SPIE
Vol. 9899, 98990S · © 2016 SPIE · CCC code: 0277-786X/16/$18 · doi: 10.1117/12.2228701

$$f_{n,vac} = \frac{\pi T}{8\sqrt{12}L^2}\sqrt{\frac{E}{\rho}}\nu_n^2 \quad (1)$$

where ρ = 2650 kg/m^3 is the density of quartz, E = 72 GPa is the quartz Young's modulus, $\nu_{n=0}$ = 1.194 for the lowest flexural mode of oscillation (fundamental mode) and $\nu_{n=1}$ = 2.988 for the first overtone mode.

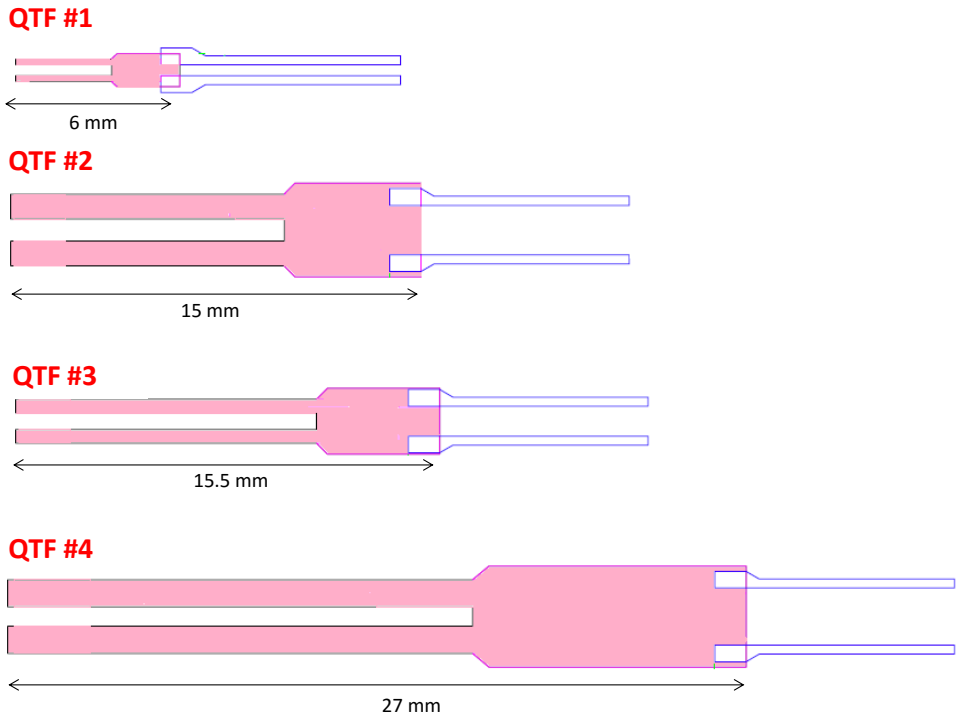

Fig. 1. Schematic view of four investigated custom QTFs in the x-z plane view.

The dimensions of the investigated QTFs and the corresponding calculated resonance frequencies are listed in Table I.

Table I. Dimensions of four custom tuning forks: L (QTF prong length), T (thickness of the prong), w (thickness of the quartz crystal) the spacing between prongs and the calculated resonance frequency for the fundamental (f_0) and the first overtone mode (f_1).

Parameters	QTF #1	QTF #2	QTF #3	QTF #4
L (mm)	3.5	10.0	11.0	17.0
w (mm)	0.25	0.25	0.25	0.25
T (mm)	0.2	0.9	0.5	1.0
Prong spacing (mm)	0.4	0.8	0.6	0.7
$f_{0, vac}$	14049.60	7230.24	3456.72	2869.09
$f_{1, vac}$	87968.59	45261.30	21639.06	18993.37

2.1 Quartz tuning fork characterization

To determine the resonance properties of the QTFs, a sinusoidal voltage is applied to the QTFs and its frequency varied by means of a function generator. The output current signal passes through a current-to-voltage converter using an operational amplifier and the generated voltage is measured by a lock-in amplifier and processed via a data acquisition card. The frequency response of the investigated QTFs was obtained with an excitation voltage level of V_0 = 0.5 mV.

The QTF in-phase current components can be written:

$$I_a = \frac{I_M (\Delta f)^2 f^2}{(\Delta f)^2 f^2 + \left(f^2 - f_{0,vac}^2\right)^2} \tag{2}$$

where f is the driving frequency and I_M is the maximum current value at the resonant frequency $f_{0,vac}$ [10]. From the fit of the resonance curves, we can extract the resonance frequency of the fundamental flexural mode $f_{0(exp)}$, the current amplitude I_M at the resonant frequency, the FWHM of the resonant curve Δf, and can calculate the quality factor $Q = f_{0(exp)}/\Delta f$ as well as the electrical resistance $R=V_0/I_M$. A representative frequency-response curve obtained for QTF#1 at a pressure of 100 torr in standard air is shown in Fig. 2(a). When a QTF operates in a viscous fluid, the effective mass increases and the resonance frequency decreases. The resonance frequency scales linearly with the pressure P of the surrounding gas as:

$$f_0 = f_{0,vac} - k_p P \tag{3}$$

where $k_p = f_{0,vac} \cdot u/(2\rho_g wT)$, $f_{0,vac}$ is the QTF resonance frequency in vacuum conditions, u is the added mass due to the presence of a fluid and ρ_g is the fluid density. In addition, fluid damping reduces the resonance quality factor Q, since the presence of the gas causes energy dissipation. A fluid damping parameter can be introduced, which is proportional to the density ρ_g and the viscosity η of the fluid. Assuming that $P \propto \rho_g$ and η does not change with P, the dependence of Q upon the gas pressure P can be described as:

$$Q(P) = \frac{Q_{vac}}{1 + Q_{vac} \cdot a \cdot \sqrt{P}} \tag{4}$$

where Q_{vac} is the quality factor of the QTF under vacuum and a is a parameter related to the QTF geometry and surrounding fluid viscosity [11].

In Fig. 2b the QTF#1 fundamental mode resonance frequency variation as a function of the surrounding gas pressure is reported. From the slope of the linear fit to the data, we obtain the k_p parameter, which for QTF#1 is -0.007 Hz/Torr. In Fig. 2c, the fundamental mode quality factor Q as a function of the pressure and the best fit obtained by using Eq. (4) is described. The QTF electrical resistance R increases as a function of the surrounding gas pressure and in Fig. 2d are shown the data obtained for QTF#1. When raising the gas pressure from100 Torr to atmospheric pressure the QTF#1 resistance changes from 700 KΩ up to 1300 KΩ. Similar behavior were observed for the other three QTF samples.

The primary noise source in QEPAS is the thermal noise associated with the QTF at the resonant frequency. The QTF thermal noise can be expressed in terms of its root mean square (rms) voltage noise:

$$\sqrt{V_{rms}^2} = R_g \sqrt{\frac{4k_b T}{R}} \sqrt{\Delta f_B} \tag{5}$$

where k_B is the Boltzmann constant, T is QTF temperature, R_g is the value of the feedback resistor of the operational amplifier, Δf_B is the detection bandwidth [12]. From eq. (5) we can determine the QTF noise level. For example, for QTF#1, with R_g = 10MΩ, for a signal integration time of 0.1 sec, corresponding to Δf = 1.6675 Hz we estimate a noise level of ~2 μV.

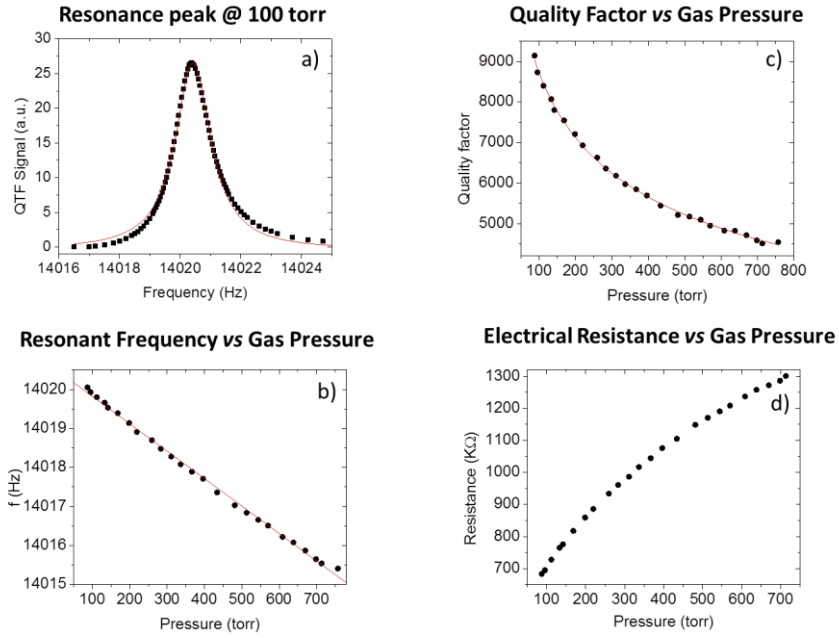

Fig. 2. a) Resonance curves of the QTF#1 current (■ symbols) measured at a pressure of 100 Torr in standard air near the fundamental oscillation mode. The red curve indicates the best-fit curve using eq. (2). b) QTF#1 resonance frequency (● symbols) measured as a function of the standard air pressure for QTF#1. Solid line is the linear fit of the data. c) Quality factor Q (● symbols) measured as a function of the standard air pressure for QTF#1. The solid red curve is the best fit obtained using Eq. (4). d) QTF#1 resistance measured as a function of the standard air pressure.

By measuring the QTF noise signal and using an Allan-Werle analysis, we can extract the experimental QTF noise level as a function of the lock-in integration time [13,14]. The data measured for the QTF#1 are shown in Fig. 3. At 0.1 sec integration time, we measure a noise level of 60,3 μV. Considering that the signal is amplified by a factor of 30 by the operational amplifier, our results are in very good agreement with the theoretical estimation. A similar behavior was observed also for the other three custom QTFs.

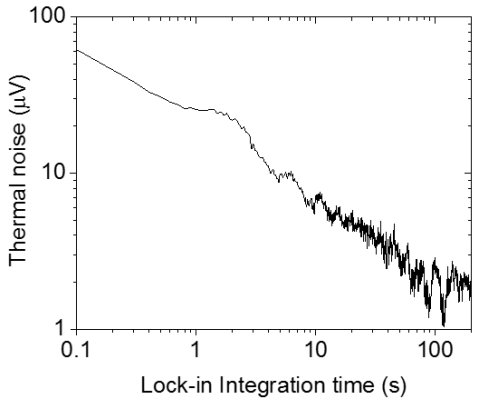

Fig. 3. Allan deviation plot measured for the QTF#1 dark-noise signal as a function of the integration time.

2.1 First overtone mode of a quartz tuning fork

The harmonic oscillator model discussed in this work applies also for the higher harmonic resonances of the prong vibrations. Hence, let us consider the first overtone mode. Its frequency increases as $f_{vac,1}=(\nu_1/\nu_0)^2 \cdot f_{0,vac} \cong 6.25 \cdot f_{0,vac}$ (see Eq. (1)). We tested our QTFs at atmospheric pressure and at a fixed excitation level of V = 0.5 mV. The measured frequency responses of the first overtone mode for QTF#2 and 4 are shown in Fig. 4.

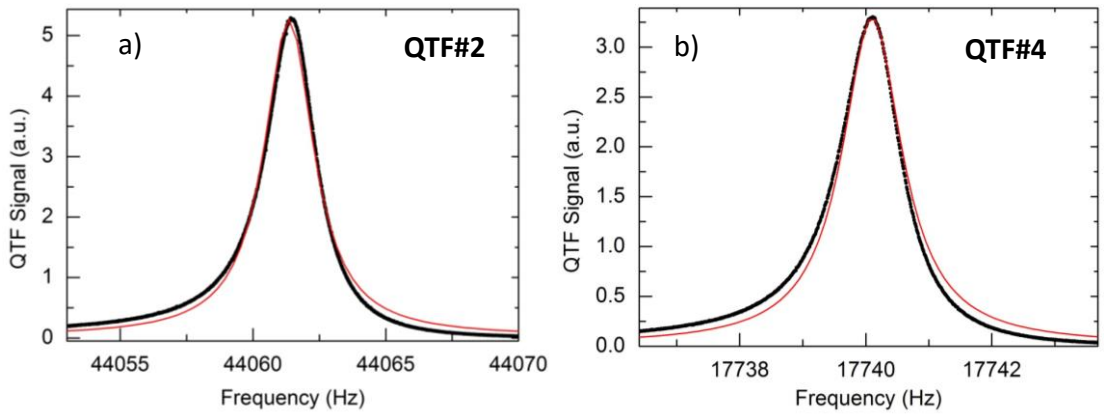

FIG. 4. Resonance curves measured for the first overtone mode of QTF#2 (a) and QTF#4 (b) as a function of the exciting frequency, at a voltage level V = 0.5 mV, in standard air and atmospheric pressure. The red curves are the best fits using eq. (2).

From these data, we can extract the f_1 first overtone resonance frequencies, the current amplitude I_M at these frequencies and the quality factor Q_1. In Table II, we report the resonance frequencies measured for the fundamental and first overtone mode and the related quality factors, for the four investigated custom QTFs at a pressure of 100 Torr.

Table II. Measured resonance frequencies for the fundamental (n = 0) and first overtone (n = 1) mode for 4 investigated QTFs.

	QTF #1	QTF #2	QTF #3	QTF #4
f_0	14020.14	7229.82	3455.86	2868.67
Q_0	9150	20250	9200	12100
f_1	86574.40	44061.35	21500.15	17740.10
Q_1	1650	10770	24530	31370

The discrepancies between experimental and theoretical values are mostly due to the damping of the gas and additional weight of the electrode gold layers [9].

An important requirement for efficient sound wave generation in QEPAS based sensor systems is to keep $f_n < 1/2\pi\tau$, where $1/\tau$ is the gas target relaxation rate. QTF resonance frequencies suitable for sensitive QEPAS based trace gas detection should be lower than 50 kHz. Electrical tests showed that for QTF#3 and #4 the first overtone vibrational mode provides a higher quality factor and increased piezoelectric current peak values, with respect to the fundamental flexural one, thus starting a new approach to exploiting QTF overtone vibrational modes for QEPAS based trace gas sensing.

With the aim to demonstrate this possibility, we implemented QTF#2, 3 and 4 in a QEPAS based sensor system operating in the near-IR spectral range. We again selected water vapor as the target gas and performed a comparison of the QEPAS signal using both the fundamental and first overtone QTF flexural modes. The optimum selected water line is located at 7299.43 cm^{-1} and has a linestrength of 1.01×10^{-20} cm/mol, according to the Hitran database [15]. A diode laser emitting at 1.37 μm was used as the excitation source and as the gas mixture we used air sampled containing a fixed 1.7% water concentration. Representative spectral scans obtained for QTF#3 at both the fundamental and first overtone QTF flexural mode are shown in Fig. 5.

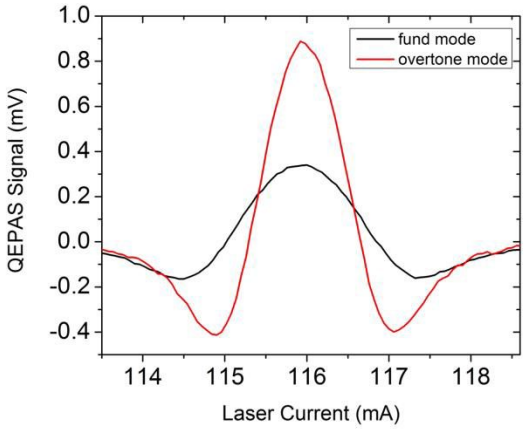

FIG. 5. QEPAS spectral scans of a gas mixture containing air with a 1.7% water concentration for the fundamental mode (black solid line) and for the first overtone one (red solid line) of the QTF#3 obtained at a gas pressure of 100 Torr.

The obtained results demonstrate that for QTF#3 and QTF#4 operating in the first overtone flexural mode is advantageous in terms of the optimum QEPAS signal, as expected considering the higher quality factor for the overtone mode, with respect to the fundamental mode.

Finally, QTF#2 and QTF#4 were recently used in QEPAS sensors employing a fiber amplified near IR laser [16] and a THz QCLs [17]. The obtained results demonstrated that the use of QTFs with prongs spacing larger than 600 μm allow adequate focalization of the excitation beam even for laser sources of limited beam quality or long wavelength (λ>60 μm) and avoids that the incident laser radiation strikes the QTF and gives rise to undesirable non-zero background signals.

3 CONCLUSIONS

In this manuscript, we reported an investigation of the electrical and QEPAS performance of four custom tuning forks, when operating at the fundamental and first overtone modes. We identified the optoacoustic gas sensing figures of merit and investigated their dependence from the QTFs relevant dimensions. The obtained results demonstrate that by an appropriate design of the QTF prong geometry, overtone vibrational modes can provide significantly higher QEPAS signals with respect to the fundamental flexural mode. In addition, the use of QTFs with a prong spacing larger than 600 μm has led to the use of THz laser sources and near-IR fiber amplified lasers, characterized by a limited laser beam quality, for QEPAS based trace gas sensing.

REFERENCES

[1] Patimisco P., Scamarcio G., Tittel F. K. and Spagnolo V., “Quartz-Enhanced Photoacoustic Spectroscopy: A Review,” Sensors 14, 6165 (2014).

[2] Kosterev A. A., Tittel F. K., Serebryakov D., Malinovsky A. and Morozov A., “Applications of quartz tuning forks in spectroscopic gas sensing,” Rev. Sci. Instrum. 76, 043105 (2005).

[3] Ren W., Jiang, W., Sanchez N. P., Patimisco P., Spagnolo V., Zah C.-E., Xie F., Hughes L. C., Griffin R. J., and Tittel F. K., “Hydrogen peroxide detection with quartz-enhanced photoacoustic spectroscopy using a distributed-feedback quantum cascade laser,” Applied Physics Letters 104, 041117 (2014).

[4] Jahjah M., Jiang W., Sanchez N. P., Ren, W., Patimisco P., Spagnolo V., Herndon S. C., Griffin R. J., and Tittel F. K., “Atmospheric CH4 and N2O measurements near Greater Houston area landfills using a QCL-based QEPAS sensor system during DISCOVER-AQ 2013,” Optics Letters 39, 957 (2014).

[5] Patimisco P., Sampaolo A., Dong L., Giglio M., Scamarcio G., Tittel F.K., and Spagnolo V., "Analysis of the electro-elastic properties of custom quartz tuning forks for optoacoustic gas sensing," Sensor and Actuators B 227, 539 (2016)

[6] Sampaolo A., Patimisco P., Dong L., Geras A., Scamarcio G., Starecki T., Tittel F.K., and Spagnolo V., "Quartz-enhanced photoacoustic spectroscopy exploiting tuning fork overtone modes," Applied Physics Letters 107, 231102 (2015)
[7] Tittel F.K., Sampaolo A., Patimisco P., Dong L., Geras A., Starecki T., and Spagnolo V., "Analysis of overtone flexural modes operation in quartz-enhanced photoacoustic spectroscopy," Optics Express 24, (2016).
[8] Lee S., Lee J.Y., and Park T.S., "Fabrication of SMD 32.768 kHz tuning fork-type crystals: Photolithography and selective etching of an array of quartz tuning fork resonators," Mater. Corros. 52, 712 (2001).
[9] Patimisco P., Borri S., Sampaolo A., Beere H.E., Ritchie D.A., Vitiello M.S., Scamarcio G., and Spagnolo V., "Quartz enhanced photo-acoustic gas sensor based on custom tuning fork and terahertz quantum cascade laser," Analyst 139, 2079 (2014).
[10] Bradley D.I., Fear M.J., Fisher S.N., Guénault A.M., Haley R.P., Lawson C.R., Pickett G.R., Schanen R., Tsepelin V. and Wheatland L.A., "Stability of flow and the transition to turbulence around a quartz tuning fork in superfluid ^{4}He at very low temperatures," Phys. Rev. B 89, 214503 (2014).
[11] Zhang W., and Turner K., "Frequency Dependent Fluid Damping of Micro/nano Flexural Resonators: Experiment, Model and Analysis," Sensors and Actuators A 134, 594 (2007).
[12] Kosterev A.A., Buerki P.R., Dong L., Reed M., Day T., Tittel F.K., "QEPAS detector for rapid spectral measurements," Appl. Phys. B 100, 173 (2010).
[13] Allan D.W., "Statistics of atomic frequency standards," Proc. IEEE 54, 221 (1966).
[14] Werle P., Miicke R., and Slemr F., "The Limits of Signal Averaging in Atmospheric Trace-Gas Monitoring by Tunable Diode-Laser Absorption Spectroscopy (TDLAS)," Appl. Phys. B 57, 131 (1993).
[15] Rothman L. S., Gordon I. E., Babikov Y., Barbe A., Chris Benner D., Bernath P. F., Birk M., Bizzocchi L., Boudon V., Brown L. R., Campargue A., Chance K., Cohen E. A., Coudert L. H., Devi V. M., Drouin B. J., Fayt A., Flaud J. M., Gamache R. R., Harrison J. J., Hartmann J. M., Hill C., Hodges J. T., Jacquemart D., Jolly A., Lamouroux J., Le Roy R. J., Li G., Long D. A., Lyulin O. M., Mackie C. J., Massie S. T., Mikhailenko S., Muller H. S. P., Naumenko O. V., Nikitin A. V., Orphal J., Perevalov V., Perrin A., Polovtseva E. R., Richard C., Smith M. A. H., Starikova E., Sung K., Tashkun S., Tennyson J., Toon G. C., Tyuterev V. G., and Wagner G., "The HITRAN2012 molecular spectroscopic database," J. Quant. Spectros. Radiat. Transfer 130, 4 (2013).
[16] Wu H., Sampaolo A., Dong L., Patimisco P., Liu X., Zheng H., Yin X., Ma W., Zhang L., Yin W., Spagnolo V., Jia S., and Tittel F.K., "Quartz enhanced photoacoustic H_2S gas sensor based on a fiber-amplifier source and a custom tuning fork with large prong spacing," Appl. Phys. Lett. 107, 111104 (2015).
[17] Spagnolo V., Patimisco P., Pennetta R., Sampaolo A., Scamarcio G., Vitiello M.S., and Tittel F.K., "THz Quartz-enhanced photoacoustic sensor for H_2S trace gas detection," Optics Express 23, 7574 (2015).